

# Angle of Arrival Estimation for Gesture Recognition from reflective body-worn tags

Sahar Golipoor, Reza Ghazalian, Inês Lobato Mesquita, and Stephan Sigg

**Abstract**—We investigate hand gesture recognition by leveraging passive reflective tags worn on the body. Considering a large set of gestures, distinct patterns are difficult to be captured by learning algorithms using backscattered received signal strength (RSS) and phase signals. This is because these features often exhibit similarities across signals from different gestures. To address this limitation, we explore the estimation of Angle of Arrival (AoA) as a distinguishing feature, since AoA characteristically varies during body motion. To ensure reliable estimation in our system, which employs Smart Antenna Switching (SAS), we first validate AoA estimation using the Multiple SIgnal Classification (MUSIC) algorithm while the tags are fixed at specific angles. Building on this, we propose an AoA tracking method based on Kalman smoothing. Our analysis demonstrates that, while RSS and phase alone are insufficient for distinguishing certain gesture data, AoA tracking can effectively differentiate them. To evaluate the effectiveness of AoA tracking, we implement gesture recognition system benchmarks and show that incorporating AoA features significantly boosts their performance. Improvements of up to 15% confirm the value of AoA-based enhancement.

**Index Terms**—Body-worn RFID, angle-of-arrival, MUSIC, Kalman smoother, gesture recognition.

## I. Introduction

**R**ADIO based human sensing comprises the analysis of electromagnetic signals reflected back from individuals or objects, with the aim of, for instance, localization [1] gesture [2], vital sign [3] or emotion recognition [4]. It is essential part of many applications including remote health monitoring, ambient assisted living, as well as smart home and factory [5]. Challenges in Radio-based human sensing exist. One primary difficulty lies in the fact that the received signal constitutes a superposition of reflections from both the target subject, such as a human, and various non-target objects present in the environment. This complicates accurate recognition and interpretation of the human-related signal components. Furthermore,

We acknowledge funding by the European Union in the frame of the Horizon Europe EIC project SUSTAIN (project no. 101071179), and Holden (project no. 101099491). Views and opinions expressed are those of the authors and do not necessarily reflect those of the European Union.

Sahar Golipoor and Stephan Sigg are with the Department of Information and Communications Engineering, Aalto University, Espoo, 02150 Finland (e-mail: {sahar.golipoor, stephan.sigg}@aalto.fi).

Reza Ghazalian is with Nokia Mobile Networks, Espoo, 02610, Finland, and also with the Department of Information and Communications Engineering, Aalto University, Espoo, 02150, Finland (e-mail: reza.ghazalian@nokia.com; ext-reza.ghazalian@aalto.fi).

Inês Lobato Mesquita is with KTH Royal Institute of Technology, SE-100 44, Stockholm, Sweden, and also the Electrical and Computer Engineering Department at Instituto Superior Técnico (e-mail: inesme@kth.se)

since a region of interest is defined for human sensing and everybody in the region could be sensed, one will find radio-based human sensing privacy invasion.

Concurrently, ultra-high frequency radio frequency identification (UHF RFID) tag, which is conventionally known for identification applications, has demonstrated its potential for sensing thanks to its low cost, contactless modality and capability of making the targets' surfaces intelligent [6] [7]. Each RFID tag contains a unique Electronic Product Code (EPC). Therefore, a potential solution to the previously mentioned challenges involves the use of smart clothing embedded with RFID tags. a) By wearing such garments, it becomes possible to determine the specific body region from which a signal is transmitted during RFID tag-reader interactions. This can enhance gesture recognition, particularly for complex gestures. b) By wearing such smart cloths, individuals who choose to be monitored can be uniquely identified, while those concerned about privacy will not be detected.

There are different sensing indicators for received signals such as time of arrival (ToA), Time Difference of Arrival (TDoA), received signal strength (RSS), phase of arrival (PoA), and phase difference of arrival (PDoA) [8].

UHF RFID works in 860-960 MHz frequency range and does not offer high bandwidth. Thus, ToA and TDoA estimation has considerable error and will not help in RFID-based sensing scenarios [9]. Besides, RSS and phase-based approaches are highly influenced via fading and multipath effects [10] and are not sufficiently robust and reliable in some scenarios. Figs. 5a and 5b, for example, show the extracted RSS and phase received from an RFID tags attached on human hand while doing different gestures. As can be seen they are relatively analogous for two different gestures and might not be solitary useful for recognition purposes. On the other hand, angular measurements are capable to provide unique information for sensing scenarios. Angle of arrival (AoA) in receiver provide knowledge from which direction signals are coming that is advantageous, particularly in target tracking applications, and real-time localization [11] [12]. In general, estimation of this indicators would be beneficial specially if they were fused with RSS or phase. Accordingly, we explore AoA tracking within a body-worn RFID system as a means to enhance gesture recognition. Our contributions are

- the estimation of AoA of tags in the azimuth direction using the MUSIC algorithm within an RFID system that employs Smart Antenna Switching.

- an enhanced performance of gesture recognition systems from body-worn reflective tags, using AoA tracking refined with a Kalman filter.
- a validation of the benefit of AoA for human gesture recognition on various benchmark models.

## II. Related Work

Popular environmental radio sensing modalities are RFID, WiFi and mmWave Radar. Particularly, the application of sign-language recognition has been prominently investigated for RFID-based recognition systems [13]–[15]. Classical machine learning (e.g. dynamic time warping (DTW), support vector machines (SVM), decision trees, random forest classifiers) have been utilized traditionally [16]–[18], but also convolutional neural networks (CNN)-based approaches [19] and data augmentation were used with good success [20].

The channel state information (CSI) in WiFi contains information on the signal strength and the phase of the received signal across multiple frequency carriers. This information can be utilized for sensing [21], using e.g. CNN [22] or graph-based neural networks [23]. A common challenge is the dependency of the recognition on the relative orientation of a subject and the WiFi device, which can be addressed by antenna placement settings [24]. Attention mechanisms have been successfully employed to improve recognition accuracy through weighing amplitude and phase features differently [25], [26].

Radar-based motion recognition has received increased attention recently and predominantly for human gesture recognition [27] exploiting range-angle, range-Doppler, range-time and angle-time maps [28], [29]. In the literature, attention mechanisms [30], interpretation of spectrogram images via image-based neural networks [31], as well as graph-based approaches [32] have been proposed to classify radar-data.

A major challenge in the aforementioned works is that the received signal is a superposition of multipath reflections and has to first be separated into the signal of interest versus reflections from environmental objects. In addition, radio sensing faces significant privacy concerns since, similar to video or audio-based systems, it is not easily possible to constrain the sensing of the system spatially or towards target groups.

We propose attaching reflective tags on-body to mitigate reflections from the environment and other subjects. Likewise, body-worn systems significantly reduce privacy issues since conscious wearing of sensors comprises an implicit consent mechanism.

RFID has been integrated into objects and tools for studies on human-object interaction or daily activities [33], customer behavior [34], capture sentiments associated with specific items [35], and observe collaborative actions in high-stakes settings like trauma resuscitation [36]. In [37], the authors advanced this concept by attaching RFID arrays to objects and leveraging orthogonal antennas for motion tracking, effectively turning physical items into interactive human-computer interfaces. Unlike these

prior approaches, which typically rely on static RFID infrastructures embedded in the environment or fixed to objects, our work introduces a dynamic system where RFID tags are embedded directly into clothing. This configuration allows the tags to move synchronously with the user's gestures. Thanks to their minimal weight and flexibility, RFID tags can be attached to garments, making them useful for applications in smart textiles and wearable technology [38], [39]. Moreover, in contrast to environmental setups, wearable RFID systems provide the added benefit of differentiating between movements of distinct body parts, as shown in our previous work [40].

In [41], we introduced a wearable RFID-based system capable of recognizing activities related to presence detection by jointly analyzing features derived from both phase and RSS signal. Prior studies have leveraged DTW for fine-grained gesture recognition, particularly through RFID tags embedded in wearable items like gloves [42], [43]. Additionally, a position-invariant method was presented in [44], where sign language recognition was achieved by normalizing key hand motion attributes such as the horizontal rotation angle and radial distance.

Employing RFID tags on the human body for coarse-grained gesture recognition introduces challenges. Frequent changes in tag orientation during movements disrupts stable signal reception by RFID readers and leads to degraded signal quality due to polarization mismatches [45]. Additionally, signal reflection is affected by anatomical features and tissue composition [46]. As a result, differences in body shape and tissue can alter reflection patterns, making it difficult to maintain distinguishable signal signatures for the same gesture, thus reducing recognition accuracy. To address these challenges, [47] proposed a multi-modal strategy for coarse-grained gesture recognition, integrating CNNs and Long Short-Term Memory (LSTM) models to extract and interpret features from RFID data. In our previous work [48], we developed two models, one based on a VGG16 architecture that leverages IQ scatter plots, and another phase-driven approach that applies segmentation via zero-crossing detection combined with a refined derivative-based technique. In contrast to the above studies, we incorporate tags' AoA tracking as new features to facilitate gesture recognition models.

Directional of arrival-based sensing outperforms ToA and TDoA by needing fewer anchors and less synchronization. Diverse techniques and algorithms for AoA finding have been reviewed in [49] in terms of theoretical foundations and computational complexity. Direction of arrival has been studied using WiFi, Radar, UWB, and RFID [50]. RFID uses backscatter communication by default, and backscatter-based UWB has also been explored in researches [51]. While UWB modules offer accurate timing for tracking and positioning, they require batteries, manual maintenance, and are hard to attach. In contrast, passive UHF RFID tags are wirelessly powered and easily embedded due to their small size and light weight.

Tags designs were conducted to perform AoA and

orientation based localization [52]–[54]. Using software defined radio (SDR), AoA was measured for Gen2 tag inventory [55], and localization [56] [57]. AoA estimation has been conducted by resolving the  $\pi$  phase ambiguity [58] and array based phase separation technique [59]. In [60], AoA estimates has been refined with deep learning on 2-dimensional feature image. To determine the direction angle, a retrieval method using coordinate system rotation [61], and mutual coupling interference [62] were investigated. AoA-based localization has been studied using frequency-scanning leaky-wave antennas [63] and sparse tag arrays [64]. Contrary to the mentioned works that employed AoA for positioning, we investigate the use of AoA tracking of wearable tags for gesture recognition.

Notation: Vectors and matrices are denoted by lowercase and uppercase bold letters, respectively. The  $i$ -th element of vector  $\mathbf{a}$  is represented by  $[\mathbf{a}]_i$ . The transpose operator is denoted by  $(\cdot)^\top$ , and the conjugate transpose (Hermitian) operator by  $(\cdot)^\text{H}$ . The  $L_2$  norm (Euclidean norm for vectors and Frobenius norm for matrices) is denoted by  $\|\cdot\|$ . The four-quadrant inverse tangent function is written as  $\text{atan}2(y, x)$ . The expectation operator is denoted by  $\mathbb{E}(\cdot)$ , and  $\mathbf{I}_2$  denotes the identity matrix of size  $2 \times 2$ .  $\text{Tr}(\mathbf{A})$  denotes the trace of the matrix  $\mathbf{A}$ , which is the sum of its diagonal elements.

### III. System and Signal Models

In this section, we introduce the RFID system model considered, together with the models of the received signals that will be used in the gesture recognition models.

#### A. System Model

Consider the RFID system scenario illustrated in Fig 1, which consists of a two-element antenna RFID reader located at a known position,  $\mathbf{p}_R \in \mathbb{R}^2$ . The system also includes one or more passive<sup>1</sup> single-antenna tags located at unknown positions. These positions are denoted as  $\mathbf{p}_i \in \mathbb{R}^2$ , where  $i \in 1, \dots, N_t$ , and  $N_t$  denotes the number of tags. The tags must be within the field of view of the RFID antennas to avoid misdetection.<sup>2</sup> The RFID reader transmits a carrier wave (CW) using right-hand circular polarization to prevent misdetection caused by polarization mismatch between the RFID reader's antennas and the tags' antennas. Additionally, we assume that the system is configured such that the tags operate within the far-field range of the RFID reader's antenna, where  $\|\mathbf{p}_R - \mathbf{p}_i\| \geq 2D^2/\lambda$  with  $D$  being the maximum dimension of the RFID reader's antenna array [65].

We utilize Alien AZ 9662 passive RFID tags, attaching two tags to the back of each hand. The setup employs an Impinj Speedway R420 RFID reader [66] and two Vulcan RFID PAR90209H antenna with 9 dBic antenna gain as well as elevation and azimuth beamwidth of 70°.

<sup>1</sup>The passive RFID tags are powered by the transmitted signal from the RFID reader.

<sup>2</sup>Tag misdetection also depends on the transmit power, which can be configured through the RFID reader's software.

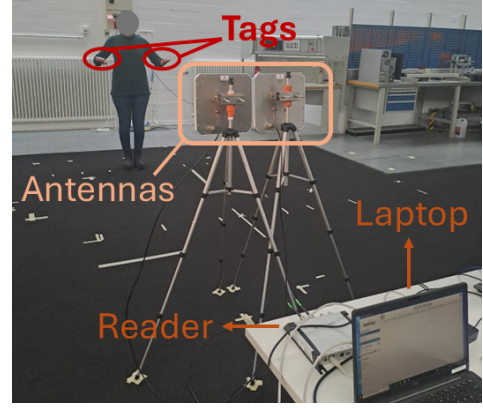


Fig. 1: Experimental setup for body-worn RFID-based gesture recognition. Two passive RFID tags are attached to the subject, with phase and RSS data collected using an Impinj Speedway R420 reader and two circularly polarized antennas.

The antennas are connected to a laptop equipped with ItemTest software, which enables communication between the reader and the RFID system.

The global coordinate system is aligned with the RFID reader's, which employs a two-element uniform linear array with elements at  $(-d/2, 0)$  and  $(d/2, 0)$ . The spacing between the elements is assumed to be  $d = 0.8\lambda$ , where  $\lambda$  is the wavelength of the carrier's frequency. The RFID reader utilizes Smart Antenna Switching (SAS) [67]. Initially, a signal is transmitted from the first antenna to detect the presence of tags within the antenna's field of view. If fewer than a predefined number of tags are detected<sup>3</sup>, the system switches to the second antenna. Otherwise, the tags found within the field of view of the first antenna are inventoried before switching to the second antenna.

#### B. Signal Model

The passive RFID tag consists of an integrated circuit (IC) and an antenna, which is made up of two distinct segments forming a dipole. During reader-tag communication, the reader transmits a CW signal, and the tag's IC harvests power from the received signal. It then modulates the response by changing the antenna's load to backscatter or absorb the wave from the reader, resulting in the reflection coefficient,  $\Gamma \in \{0, 1\}$ .<sup>4</sup> The RFID system is a SAS system and samples the backscattered signal from the tag(s) at each antenna element at different times, but periodically.

<sup>3</sup>The reader software provides an option to set the upper limit on the number of tags that can be detected.

<sup>4</sup>The reflection coefficient is calculated as :  $\Gamma = \frac{Z_{\text{Ant}} - Z_{\text{Load}}}{Z_{\text{Ant}} + Z_{\text{Load}}}$ , where  $Z_{\text{Ant}}$  and  $Z_{\text{Load}}$  denote the antenna impedance (typically around  $50\Omega$ ) and the load impedance controlled by the tag's IC, respectively. When  $Z_{\text{Load}}$  is matched with  $Z_{\text{Ant}}$ , i.e.,  $Z_{\text{Load}} = Z_{\text{Ant}}$ , then  $\Gamma = 0$ , meaning that there is no reflection. If the  $Z_{\text{Load}} = 0$ , i.e., a shortcut circuit, then  $\Gamma = 1$ . In practice, due to imperfect load matching, the maximum value of the  $\Gamma$  is close to 1 and the minimum value is close to zero.

The spatially sampled signals from each antenna are down-converted to a lower frequency using the oscillator and low-pass filter. These signals are subsequently fed into the analog-to-digital converter (ADC) to extract the in-phase and quadrature (IQ) components. The reader's system is based on a single transceiver card, meaning that a common oscillator is used for both transmission and reception. As a result, there will be no frequency offset in the baseband signal (IQ samples).

The AoA in the azimuth direction of the line-of-sight (LoS) path from the  $i$ -th tag relative to the center of the reader's antenna array is calculated as  $\theta_i = \text{atan2}([\mathbf{q}_i]_2, [\mathbf{q}_i]_1) - \pi/2$ , where  $\mathbf{q}_i = \frac{\mathbf{p}_i - \mathbf{p}_R}{\|\mathbf{p}_i - \mathbf{p}_R\|}$ . Similarly, the AoA of the  $\ell$ -th non-line-of-sight (NLoS) path associated with the  $i$ -th tag, which originates from the  $\ell$ -th scatterer located at  $\mathbf{p}_{s_\ell}$ , is computed as  $\theta_i^\ell = \text{atan2}([\mathbf{q}_i^\ell]_2, [\mathbf{q}_i^\ell]_1) - \pi/2$ , where  $\mathbf{q}_i^\ell = \frac{\mathbf{p}_{s_\ell} - \mathbf{p}_R}{\|\mathbf{p}_{s_\ell} - \mathbf{p}_R\|}$ . Therefore, under the above assumptions, the received signal at the  $m$ -th antenna of the reader, backscattered from the  $i$ -th tag, is denoted by  $y_{m,i}(k) \in \mathbb{C}$  as:

$$y_{m,i}(k) = g_i \sqrt{P} a_m(\theta_i) s_m(k) + \sum_{\ell=1}^L g_i^\ell \sqrt{P} a_m(\theta_i^\ell) s_m(k) + \nu_{m,i}(k), \quad \forall m, i \in \{1, 2\}, \forall k \in \{1, 2, \dots, K\} \quad (1)$$

where  $g_i$  and  $g_i^\ell$  represent the channel gains of the round-trip path between the reader and the  $i$ -th tag for the LoS and the  $\ell$ -th NLoS paths, respectively.  $s_m(k) = x(4k+2m+i-6)$  is the transmit signal over  $m$ -th antenna at time  $k$ , and  $x(k) = e^{j2\pi f_c k T_s}$ ,  $f_c$  is the carrier frequency of the transmitted signal from the reader,  $T_s$  is the sampling period of the ADC.  $\nu_{m,i}(k)$  indicates the effect of additive thermal noise at the reader, modeled as a zero-mean Gaussian distribution with variance  $\sigma^2$ .  $P$  is the transmit power at the reader in the transmission mode.  $L$  denotes the total number of NLoS paths. The  $m$ -th element of the steering vector is expressed as  $a_m(\theta_i) = \exp(j \frac{4\pi d}{\lambda} (m-1) \sin(\theta_i)) \quad \forall m \in \{1, 2\}$ .<sup>5</sup> We assume that the NLoS paths are weaker than the LoS path, which allows us to focus on the tag's AoA estimation in the subsequent step. Thus, we rewrite (1) as

$$y_{m,i}(k) = g_i \sqrt{P} a_m(\theta_i) s_m(k) + \nu'_{m,i}(k), \quad (2)$$

$$\forall m, i \in \{1, 2\}, \forall k \in \{1, 2, \dots, K\},$$

where  $\nu'_{m,i}(k) \triangleq \sum_{\ell=1}^L g_i^\ell \sqrt{P} a_m(\theta_i^\ell) s_m(k) + \nu_{m,i}(k)$  represents the aggregated interference from NLoS paths and additive noise.

For the next step, we concatenate all the observations from each antenna element, as given in (2), over the observation time, i.e.,  $k \in \{1, \dots, K\}$ . Thus, we have:

<sup>5</sup>Unlike the standard steering vector mentioned in the literature, which is  $a_m(\theta_i) = \exp(j \frac{2\pi d}{\lambda} (m-1) \sin(\theta_i)) \quad \forall m \in \{1, 2\}$ , the phase difference in the considered system is twice that of the one mentioned in the literature. This is due to the round-trip path between the reader and the tag.

$$\mathbf{Y}_i = g_i \sqrt{P} \mathbf{A}(\theta_i) \mathbf{S} + \mathbf{N}_i \quad \forall i \in \{1, 2\}, \quad (3)$$

where  $\mathbf{Y}_i = \begin{bmatrix} \mathbf{y}_{1,i}^\top \\ \mathbf{y}_{2,i}^\top \end{bmatrix} \in \mathbb{C}^{2 \times K/4}$ ,  $\mathbf{A}(\theta_i) = \text{diag}(\mathbf{a}(\theta_i)) \in \mathbb{C}^{2 \times 2}$ ,  $\mathbf{a}(\theta_i) = [1 \ \exp(j \frac{4\pi d}{\lambda} (m-1) \sin(\theta_i))]^\top$ ,  $\mathbf{S} = \begin{bmatrix} \mathbf{s}_{1,i}^\top \\ \mathbf{s}_{2,i}^\top \end{bmatrix} \in \mathbb{C}^{2 \times K/4}$ , where  $\mathbf{s}_{1,i}$  and  $\mathbf{s}_{2,i}$  are the transmit signals over the first and second antennas to the  $i$ -th tag, respectively. Also,  $\mathbf{y}_{1,i} \in \mathbb{C}^{K/4}$  and  $\mathbf{y}_{2,i} \in \mathbb{C}^{K/4}$  represent all the IQ samples from the first and second antenna elements from the  $i$ -th tag, respectively, over the observation time. Similarly,  $\mathbf{N}_i = \begin{bmatrix} \boldsymbol{\nu}'_{1,i}^\top \\ \boldsymbol{\nu}'_{2,i}^\top \end{bmatrix} \in \mathbb{C}^{2 \times K/4}$ , where  $\boldsymbol{\nu}'_{1,i} \in \mathbb{C}^{K/4}$  and  $\boldsymbol{\nu}'_{2,i} \in \mathbb{C}^{K/4}$  denote all the interference and noise samples from the first and second antenna elements during the reception from the  $i$ -th tag, respectively, over the observation time.

#### IV. Problem formulation and Proposed Method

In this section, we describe two main scenarios: first where one or two fixed tags are within the field of view of the readers, and another where the tag(s) are attached to the human body and move while performing gestures. In both scenarios, the goal is to estimate the AoA of the backscattered signal from the tags.

##### A. Fixed Tag(s)

In this scenario, we first consider a single tag located at an unknown AoA with respect to the center of the reader's antenna. For multiple tags, the problem can be treated as independent single-tag AoA estimations since the reader's software provides separate IQ samples for each tag, as mentioned earlier. In some cases, a tag's backscattered signal is detected by only one of the two antennas during part of the observation period. In such cases, the signal from the other antenna is discarded, because keeping it would make AoA estimation inaccurate.

1) MUSIC Algorithm: For AoA estimation, we apply the MUltiple SIgnal Classification (MUSIC). After preprocessing the IQ samples and extracting the data corresponding to the target tag (in the case of multiple tags), we obtain the concatenated measurements as given in (3). Since the signal is wide-sense stationary (WSS) and satisfies the second-order ergodicity condition<sup>6</sup>, the covariance matrix  $\hat{\mathbf{R}}_i \in \mathbb{C}^{2 \times 2}$  of  $\mathbf{Y}_i$  is estimated as:

$$\hat{\mathbf{R}}_i \triangleq \frac{1}{K/4} \mathbf{Y}_i \mathbf{Y}_i^\mathsf{H} \stackrel{(a)}{=} \alpha \mathbf{A}(\theta_i) \mathbf{R}_{ss}^i \mathbf{A}^\mathsf{H}(\theta_i) + \mathbf{R}_n^i, \quad (4)$$

where  $\mathbf{R}_{ss}^i \triangleq \frac{1}{K/4} \mathbf{S} \mathbf{S}^\mathsf{H}$ ,  $\alpha \triangleq g_i^2 P$ , and  $\mathbf{R}_n^i \triangleq \frac{1}{K/4} \mathbf{N}_i \mathbf{N}_i^\mathsf{H}$ . (a) indicates that the noise and the signal are uncorrelated. Next, we perform eigen decomposition on  $\hat{\mathbf{R}}_i$ :

$$\hat{\mathbf{R}}_i \mathbf{u}_r = \lambda_r \mathbf{u}_r, \quad \forall r \in \{n, s\}, \quad (5)$$

<sup>6</sup> $\hat{\mathbf{R}}_i \triangleq \mathbb{E}\{\mathbf{Y}_i \mathbf{Y}_i^\mathsf{H}\} \approx \frac{1}{K/4} \mathbf{Y}_i \mathbf{Y}_i^\mathsf{H}$

In which  $\mathbf{u}_r$  is the eigenvector corresponding to the eigenvalue  $\lambda_r$ , with  $\mathbf{u}_n < \mathbf{u}_s$ . Typically, eigenvectors associated with smaller eigenvalues ( $\mathbf{u}_n$ ) and larger eigenvalues ( $\mathbf{u}_s$ ) correspond to the noise subspace and signal subspace, respectively, which are orthogonal to each other. Considering these two orthogonal subspaces, we define the spectrum function, known as the MUSIC estimator, as follows [68, Eq. (6)]:

$$P_{\text{MUSIC}}(\theta_i) = \frac{1}{\mathbf{a}^H(\theta_i)\mathbf{u}_n\mathbf{u}_n^H\mathbf{a}(\theta_i)}. \quad (6)$$

Finally, we can find the peak of  $P_{\text{MUSIC}}$ , which corresponds to the AoA of the  $i$ -th tag, by performing a line search over  $[\theta_{\min}, \theta_{\max}]$ , where these values are defined based on our system's field of view. Indeed, our system's field of view is limited because the distance between the antennas is greater than  $\lambda/2$ , which leads to ambiguity in the AoA estimation.<sup>7</sup>

## B. Moving tags attached to the Human Body

In this scenario, we aim to track the AoA of the backscatter signals originating from moving tag(s) attached to the human body. To achieve this, similar to the previous section, we collect all IQ samples over the duration of the tags' movement. We then preprocess them, which includes extracting the IQ samples from each antenna for each tag, and discarding the samples measured at only one antenna for a period while the other antenna is missing, as discussed in the previous section.

Next, for each tag, we segment the pre-processed IQ samples into windows without overlap. We then estimate the AoA for each windowed IQ sample using the MUSIC algorithm, as explained in Sec. IV-A. Hence, we have  $\mathbf{z} = [\hat{\theta}_1, \hat{\theta}_2, \dots, \hat{\theta}_T]^T$ , where  $T$  is the number of windows. However, some measurements are missing due to tag misdetection during gesture execution. Therefore, we apply a Kalman smoother to the AoAs estimated by MUSIC, leveraging the system dynamics. The smoother leverages future measurements to further refine past estimates. We describe the Kalman smoother in the following sections.

Let  $\boldsymbol{\theta}_t = [\theta_i^t, \omega_i^t]^T$  represent the state of the dynamics of the changing AoA at  $t$ -th window (during the  $i$ -th tag movement), where  $\omega_i^t$  is the rate of change of the AoA, assumed to be constant. Therefore, the state and measurement equations can be expressed as follows:

$$\boldsymbol{\theta}_t = \mathbf{F}\boldsymbol{\theta}_{t-1} + \mathbf{w}_t, \quad (7)$$

$$z_t = \mathbf{H}\boldsymbol{\theta}_t + v_t, \quad (8)$$

where  $z_t \in \mathbb{R}$  denotes the measurement at  $t$ -th window,  $\mathbf{F} \triangleq \begin{bmatrix} 1 & \Delta t \\ 0 & 1 \end{bmatrix}$  denotes the dynamic matrix,  $\mathbf{H} \triangleq [1 \ 0]$  is the measurement matrix, and interval  $\Delta t$  represents the time difference between two consecutive windows.  $\mathbf{w}_t$

<sup>7</sup>Despite this limitation, the system setup is configured such that the AoA of the tag, resulting from gesture execution, falls within the unambiguous AoA range.

and  $v_t$  are the process noise and measurement noise, respectively, which are assumed to follow a Gaussian distribution with zero mean and covariance  $\mathbf{Q} = \begin{bmatrix} \sigma_\theta^2 & 0 \\ 0 & \sigma_v^2 \end{bmatrix}$  and variance  $\sigma_v^2$ , and they are assumed to be independent. A Kalman smoother has the following steps:

1) Prediction: In this step, the prior state estimate  $\hat{\boldsymbol{\theta}}_t^-$  is obtained based on the considered dynamic system given in (7) as:

$$\hat{\boldsymbol{\theta}}_t^- = \mathbf{F}\hat{\boldsymbol{\theta}}_{t-1}. \quad (9)$$

According to (9), the covariance of the error of the predicted (prior) state estimate  $\hat{\boldsymbol{\theta}}_t^-$ , i.e.,  $\mathbf{P}_t^-$ , can be calculated as:

$$\mathbf{P}_t^- \triangleq \mathbb{E}\{e_t^- e_t^{-\top}\} = \mathbf{F}\mathbf{P}_{t-1}\mathbf{F}^\top + \mathbf{Q}, \quad (10)$$

where  $e_t^- \triangleq \boldsymbol{\theta}_t - \hat{\boldsymbol{\theta}}_t^-$ ,  $\boldsymbol{\theta}_t$  is the true state at  $t$ -th window, and  $\mathbf{P}_{t-1}$  is the covariance of the error of the a posteriori state estimate  $\hat{\boldsymbol{\theta}}_{t-1}$  at  $(t-1)$ -th window, which is explained in the next step. Note that we initialize the covariance of the predicted state error at the first window as  $\mathbf{P}_0 = \mathbf{I}_2$ .

2) Measurements Update: In this step, we estimate the a posteriori  $\hat{\boldsymbol{\theta}}_t$ , based on the measurement available,  $z_t$ , provided by MUSIC in the current time window, and the prior state estimate, as follows:

$$\hat{\boldsymbol{\theta}}_t = \hat{\boldsymbol{\theta}}_t^- + \mathbf{k}_t (z_t - \mathbf{H}\hat{\boldsymbol{\theta}}_t^-), \quad (11)$$

where  $\mathbf{k}_t \in \mathbb{R}^2$  is the Kalman gain in the  $t$ -th window, obtained by minimizing the mean squared a posteriori estimation error, i.e., the trace of the a posteriori error covariance matrix,  $\mathbf{P}_t \triangleq \mathbb{E}\{e_t e_t^\top\}$ , with  $e_t \triangleq \boldsymbol{\theta}_t - \hat{\boldsymbol{\theta}}_t$ , as follows [69, Eq. (15)]:

$$\frac{d\text{Tr}(\mathbf{P}_t)}{d\mathbf{k}_t} = 0 \Rightarrow \mathbf{k}_t = \mathbf{P}_t^- \mathbf{H}^\top (\mathbf{H}\mathbf{P}_t^- \mathbf{H}^\top + \sigma_v^2)^{-1}, \quad (12)$$

where  $\mathbf{P}_t$  is updated as:

$$\mathbf{P}_t = (\mathbf{I} - \mathbf{k}_t \mathbf{H}) \mathbf{P}_t^-. \quad (13)$$

The above two steps (prediction and measurement update) are repeated sequentially until the estimate is updated based on the final AoA measurement corresponding to the last time window. Moreover, all prior and a posteriori state estimations, along with their covariance errors, are stored. This means that:

$$\hat{\boldsymbol{\Theta}} = [\hat{\boldsymbol{\theta}}_1, \hat{\boldsymbol{\theta}}_2, \dots, \hat{\boldsymbol{\theta}}_T], \quad (14)$$

$$\boldsymbol{\Theta}^- = [\hat{\boldsymbol{\theta}}_1^-, \hat{\boldsymbol{\theta}}_2^-, \dots, \hat{\boldsymbol{\theta}}_T^-], \quad (15)$$

$$\mathbf{P} = [\mathbf{P}_1, \mathbf{P}_2, \dots, \mathbf{P}_T], \quad (16)$$

$$\mathbf{P}^- = [\mathbf{P}_1^-, \mathbf{P}_2^-, \dots, \mathbf{P}_T^-]. \quad (17)$$

Note that, when no measurement is available due to tag misdetection, the Measurement Update step will be skipped for that.

3) Smoother: Next, we refine the above estimates by utilizing both future and past measurements through the Kalman filter's estimation. To achieve this, we perform the refinement in a backward direction, starting from the last window  $T$ . The backward recursion is given by [70, Eq. (12.6)]:

$$\mathbf{g}_t = \mathbf{P}_t \mathbf{F}^\top [\mathbf{P}_{t+1}^-]^{-1}, \quad (18)$$

$$\hat{\boldsymbol{\theta}}_t^s = \hat{\boldsymbol{\theta}}_t + \mathbf{g}_t (\hat{\boldsymbol{\theta}}_{t+1}^s - \hat{\boldsymbol{\theta}}_{t+1}^-), \quad (19)$$

$$\mathbf{P}_t^s = \mathbf{P}_t + \mathbf{g}_t (\mathbf{P}_{t+1}^s - \mathbf{P}_{t+1}^-) \mathbf{g}_t^\top, \quad (20)$$

where  $\mathbf{g}_t \in \mathbb{R}^2$  is the smoothing gain,  $\hat{\boldsymbol{\theta}}_t^s$  is the smoothed state estimation, and  $\mathbf{P}_t^s$  is the covariance error of the smoothed state estimate. We also initialize the smoothed state estimate and the covariance error of the smoothed state estimate as  $\hat{\boldsymbol{\theta}}_T^s = \hat{\boldsymbol{\theta}}_T$  and  $\mathbf{P}_T^s = \mathbf{P}_T$ , respectively. Overall, the proposed method for AoA tracking can be summarized as described in Algorithm 1.

## V. Results and Discussion

In this section, we evaluate the performance of the proposed algorithm. In our experiment, we set the transmit power at the reader to  $P = 30$  dBm. The maximum sensitivity is set to  $-84$  dBm. All these settings are configured via the RFID reader's software (see more details about the RFID reader's software in [71]). The distance between the line where the tag(s) with an unknown AoA are placed and the line where the RFID antennas are located is 3 m, fulfilling the far-field assumption. The reader transmits a signal with a carrier frequency of  $f_c = 865.7$  MHz, corresponding to a wavelength of  $\lambda = 34.65$  cm.

### A. AoA estimation for Fixed Tags

In this section, we demonstrate that it is possible to estimate the AoA based on the data captured by an RFID reader. We consider two scenarios for our evaluation: one with a single tag and another with two tags.

1) One Tag: In this case, we place the tag at different angles and compare the estimated and true values in two environments: the anechoic chamber and the industrial laboratory, as shown in Fig. 2. This figure presents five experiments for each environment, highlighting the best result. As observed, the estimation error in the industrial laboratory is larger compared to that in the anechoic chamber due to the multipath effect. For example, as shown in Fig. 2c, when the tag is located at  $\theta = 15^\circ$ , the AoA estimation error is approximately  $1.35^\circ$  for the anechoic chamber and  $3.58^\circ$  for the industrial laboratory. For  $\theta = 0^\circ$ , as shown in Fig. 2b, the AoA estimation error in the industrial laboratory is significantly higher, approximately  $6^\circ$ . The main reason is the presence of a strong non-line-of-sight path around  $0^\circ$ . Note that some errors arise from the setup process, including aligning the RFID reader's antenna and positioning the tags precisely. However, the results demonstrate that the AoA estimator performs reasonably well for AoA tracking in gesture recognition, which will be discussed later.

---

### Algorithm 1: AoA Tracking

---

Require: Received IQ samples,  $\mathbf{Q}$ ,  $\sigma_v^2$ ,  $\mathbf{F}$ ,  $\mathbf{P}_0$ ,  $T$ ,  $\theta_{\min}$  and  $\theta_{\max}$   
1: Extract the number of tags,  $N_t$ , from the data.  
for  $i = 1$  to  $N_t$  do  
    Pre-processing  
    2: Extract and store the IQ samples at each antenna from  $i$ -th tag. Discard the samples from one antenna when the other antenna's samples are missing.  
    AoA Measurements  
    3: Segment the samples into  $T$  non-overlapping windows.  
    for  $t = 1$  to  $T$  do  
        4.1: Estimate the covariance matrix  $\hat{\mathbf{R}}_i$  for the  $t$ -th window using (4).  
        4.2: Calculate the noise subspace of  $\hat{\mathbf{R}}_i$  using eigen decomposition given in (5).  
        4.3: Estimate  $\hat{\boldsymbol{\theta}}_t$  by finding the peak of  $P_{\text{MUSIC}}$  given in (6) via a search over  $\theta \in [\theta_{\min}, \theta_{\max}]$ .  
    end for  
    5: Store all the AoA measurements, i.e.,  
 $\mathbf{z} = [\hat{\theta}_1, \hat{\theta}_2, \dots, \hat{\theta}_T]^\top$ .  
    Kalman Filtering  
    for  $t = 1$  to  $T$  do  
        6.1 (Prediction): Estimate the prior state estimate  $\hat{\boldsymbol{\theta}}_t^-$  and calculate  $\mathbf{P}_t^-$  using (9) and (10), respectively.  
        6.2 (Measurements Update):  
            Calculate the Kalman gain  $\mathbf{k}_t$  using (12)  
            Estimate a posteriori state  $\hat{\boldsymbol{\theta}}_t$  using (11)  
            Calculate  $\mathbf{P}_t$  using (13).  
    end for  
    7: Store all prior state and a posteriori state estimations, along with their covariance errors, i.e.,  $\hat{\boldsymbol{\Theta}}$ ,  $\hat{\boldsymbol{\Theta}}^-$ ,  $\mathbf{P}$ , and  $\mathbf{P}^-$  given in (14)–(17).  
    Kalman Smoother  
    8: Set  $\hat{\boldsymbol{\theta}}_T^s = \hat{\boldsymbol{\theta}}_T$  and  $\mathbf{P}_T^s = \mathbf{P}_T$ .  
    for  $t = T$  to 1 do  
        9: Calculate the smoother gain  $\mathbf{g}_t$  using (18).  
        10: Estimate the smoothed state  $\hat{\boldsymbol{\theta}}_t^s$  using (19).  
        11: Calculate  $\mathbf{P}_t^s$  using (20).  
    end for  
    12: Store the AoA estimations for  $i$ -th tag, i.e.,  
 $\hat{\boldsymbol{\psi}}_i^s = [\hat{\boldsymbol{\theta}}_1^s[1], \hat{\boldsymbol{\theta}}_2^s[1], \dots, \hat{\boldsymbol{\theta}}_T^s[1]]^\top$   
end for  
return  $\hat{\boldsymbol{\Theta}}^s = [\hat{\boldsymbol{\psi}}_1^s, \hat{\boldsymbol{\psi}}_2^s, \dots, \hat{\boldsymbol{\psi}}_{N_t}^s]$

---

2) Two Tags: Fig. 3 demonstrates the AoA estimation where there are two tags at different angles backscattering signals. As observed, the AoA estimation error in the industrial laboratory is still acceptable compared to that in the anechoic chamber (for example, at angle  $-10^\circ$ , the error is  $3.45^\circ$  in the industrial laboratory with the presence of multipath, compared to the error of  $0.9^\circ$  in the anechoic chamber). This validates the AoA measurements

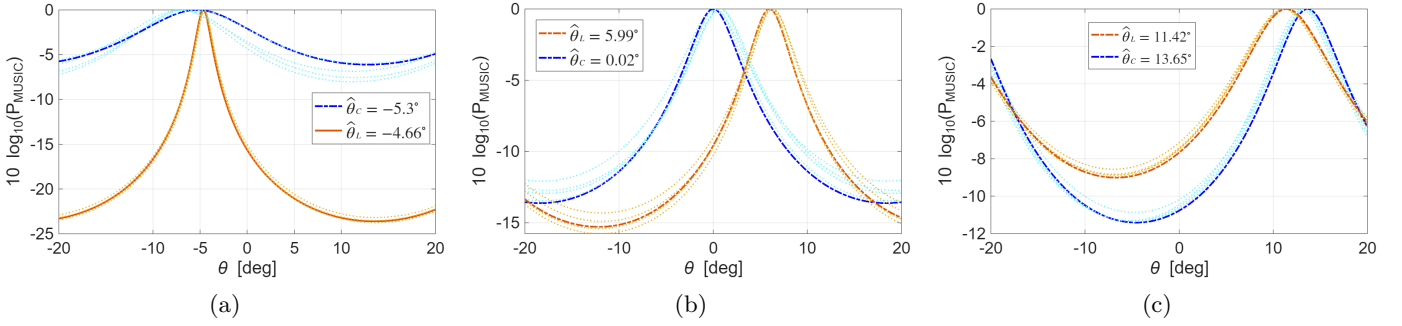


Fig. 2: The evaluation of the MUSIC algorithm for AoA estimation is conducted for a fixed tag in the anechoic chamber ( $\theta_c$ ) and in the industrial laboratory ( $\theta_L$ ) when the tag is located at: (a)  $\theta = -5^\circ$ , (b)  $\theta = 0^\circ$ , and (c)  $\theta = 15^\circ$ .

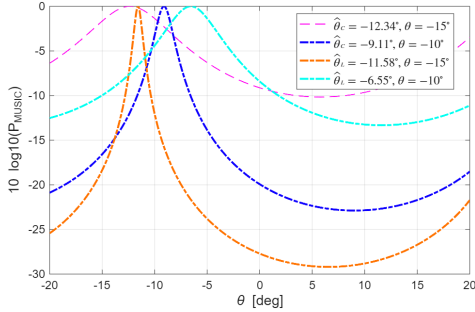


Fig. 3: The evaluation of AoA estimation with two tags, located at  $-15^\circ$  and  $-10^\circ$ , in the anechoic chamber and the industrial laboratory.

for tracking in the case of multiple tags.

#### B. AoA tracking as a complementary feature for gesture differentiation

For data collection, participants were positioned 3 meters away from the antennas. The experiment included 5 participants (2 males, 3 females) with diverse body types and heights ranging from 155 cm to 185 cm. Each participant repeated every gesture 20 times. With a total of 21 unique gestures, the resulting dataset consisted of 2100 samples. As illustrated in Fig. 4, the gestures included simple one-handed and complex two-handed movements.

Fig. 5 illustrates the advantages of AoA tracking in a gesture recognition system. Fig. 5a presents the RSS values extracted for the simple one-handed gesture set. RSS is known to be highly sensitive to environmental factors such as multipath fading, shadowing, and interference. As shown, the RSS signals for different gestures are largely indistinguishable, indicating that RSS alone is not a reliable metric for robust gesture recognition. In contrast, phase information is generally considered more reliable in RF sensing applications, as it captures fine-grained characteristics of wave propagation, including timing and path differences. However, our experimental results indicate that the phase of backscattered signals from the tags often exhibits similarities across different gestures, as demonstrated in Fig. 5b. For instance, while the phase signals for the SL and SR gestures appear quite

similar, their AoA estimations are markedly different, as shown in Fig. 5c. Specifically, the estimated AoA for the SL begins in the negative range and moves toward the positive, whereas for SR, it starts near zero, shifts briefly toward the positive, and then trends negative—consistent with the expected motion of these two gestures. Another example can be seen with the L and RAC gestures, which are not sufficiently distinguishable based on phase alone. However, when AoA is taken into account, these gestures become clearly separable. Fig. 5d displays the estimated AoA from both tags for the complex two-handed gesture set. As an illustration, the 2HLR and 2HLD gestures exhibit AoA tracks in opposite directions, despite the gestures appearing similar in execution. Likewise, the 2HIC and 2HOC gestures produce distinct AoA signal trends, even though they are performed similarly. This analysis confirms that, while RSS and phase may lack the discriminatory power required for accurate gesture recognition, AoA tracking provides spatial information that enhances recognition performance. Accordingly, the following section presents a comprehensive evaluation demonstrating the effectiveness of AoA features, both individually and when integrated with RSS and phase data, across various recognition models.

#### C. Gesture recognition using tracked AoAs

In this section, we evaluate AoA tracking in gesture recognition and demonstrate how this metric enhances the performance of various models compared to using only RSS and phase signal.

We applied benchmark approaches. We implemented Reactor [17], which extracts features from the signal and trains a Random Forest Classifier (RFC). We also employed a Support Vector Machine (SVM) [72] as an alternative classifier. For each feature configuration, RFC and SVM models were trained independently. For brevity, we denote them using RFC/SVM, referring to two separate models per configuration. Based on different feature extraction strategies from the available metrics, RSS, phase, and AoA, we constructed models as detailed below:

- RFC/SVM with SP utilizes only statistical features extracted from the phase.

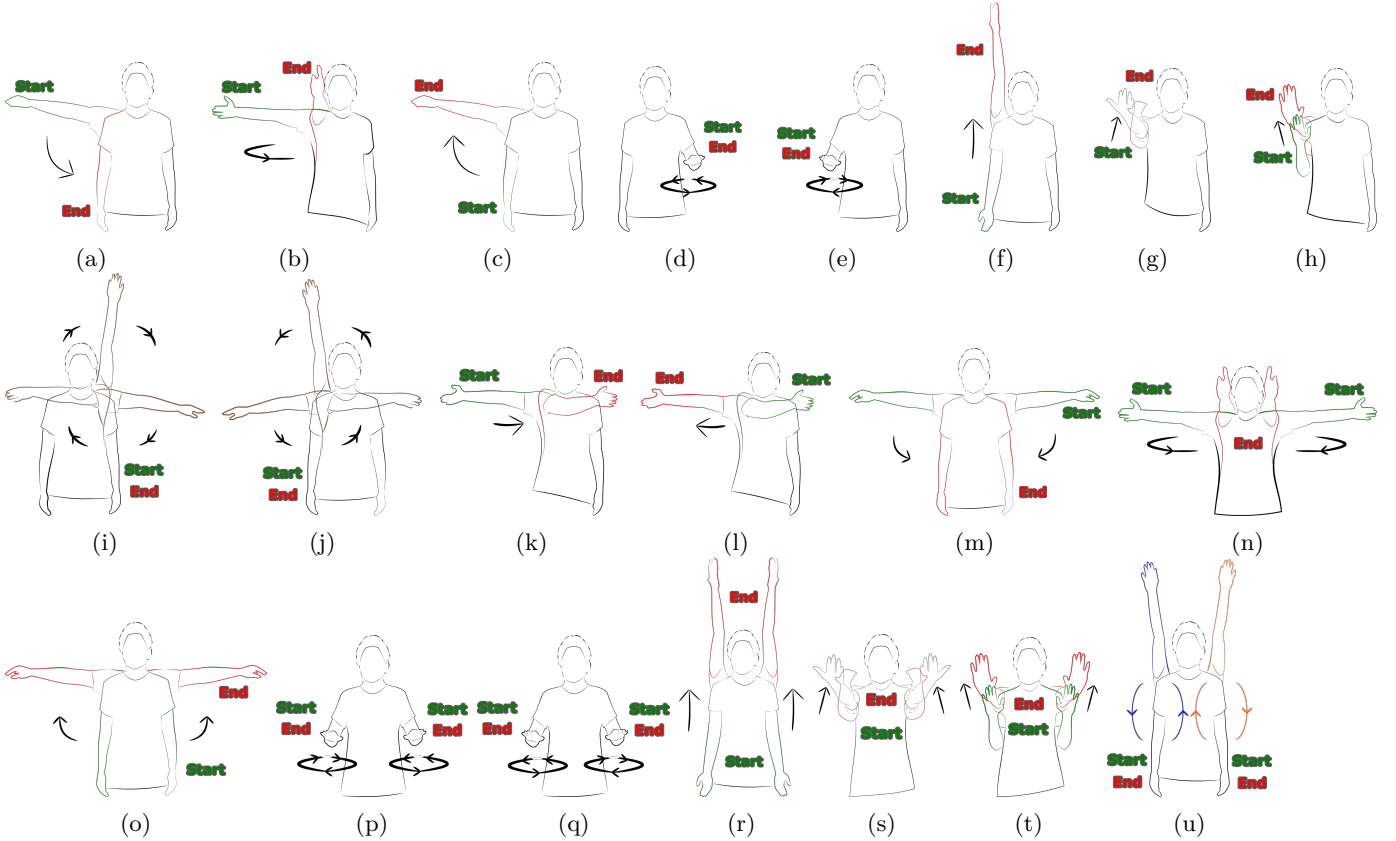


Fig. 4: The gestures performed by participants are (a) LD: Lateral Down (1), (b) LF: Lateral to Front (2), (c) LR: Lateral Raise (3), (d) LAC: Left Arm Circle (4), (e) RAC: Right Arm Circle (5), (f) L: Lift (6), (g) Pl: Pull (7), (h) Ps: Push (8), (i) LRo: Left Round (9), (j) RR: Right Round (10), (k) SL: Swipe Left (11), (l) SR: Swipe Right (12), (m) 2HLD: Two Hands Lateral Down (13), (n) 2HLF: Two Hands Lateral to Front (14), (o) 2HLR: Two Hands Lateral Raise (15), (p) 2HIC: Two Hands Inward Circle (16), (q) 2HOC: Two Hands Outward Circle (17), (r) 2HL: Two Hands Lift (18), (s) 2HPl: Two Hands Pull (19), (t) 2HPs: Two Hands Push (20), (u) 2HR: Two Hands Round (21).

- RFC/SVM with SWP combines statistical features and wavelet coefficients derived from the phase.
- RFC/SVM with SPR includes statistical features extracted from both the phase and RSS.
- RFC/SVM with SA uses only statistical features extracted from AoA.
- RFC/SVM with SWA combines statistical features and wavelet coefficients derived from AoA.
- RFC/SVM with SPRA incorporates statistical features extracted from the phase, RSS, and AoA.

We extract statistical features from signals, i.e., RSS, phase, and AoA, including the mode, the median, the first quartile, the third quartile, the mean, the max, the min, the range, the variance, the standard deviation, the third-order central moment, the kurtosis, the skewness, and the entropy. On top of that, Pearson correlations are extracted between every pair of RSS, phase, and AoA data corresponding to the two tags. Moreover, we use discrete wavelet transform with Daubechies wavelet and extract low-frequency coefficients and concatenate them to statistical features.

In addition, AoA tracking was evaluated using other

benchmark models, including the Early Fusion approach presented in [73], in which each tag's RSS and phase from both antennas, along with the AoAs corresponding to the two tags, are fed in parallel to its network. The Late Fusion method described in [41] and the EUIGR method [47] are also applied, in which features from the signals are first extracted through their respective networks and then merged. Additionally, GRfid [18], which is a dynamic time warping-based algorithm, is utilized for either phase or AoA separately.

The performance metrics, including accuracy, precision, recall, and F1-score, are presented in TABLE. I for models that use phase or phase combined with RSS as input features, and in TABLE. II for models that use AoA or its combination with phase and RSS as input features. In general, incorporating AoA leads to a notable improvement in all metrics across all methods. For example, the accuracy of the RFC model using statistical features from phase and RSS is 85.49% in TABLE. I. However, when statistical features from AoA are added, i.e., RFC with SPRA, the accuracy increases substantially to 97.2%. Similarly, the SVM-based model achieves 78.11% without AoA, while

TABLE I: Accuracy (Acc.), Precision (Pre.), Recall (Rec.), and F1-score (F1) of methods using phase and RSS inputs, excluding AoA.

Metric \ Method	Acc.	Pre.	Rec.	F1
RFC with SP	82.18	82.67	82.18	82.06
RFC with SWP	84.22	84.79	84.22	84.18
RFC with SPR	85.49	85.74	85.48	85.35
SVM with SP	75.06	76.3	75.06	75.15
SVM with SWP	79.89	80.62	79.89	79.69
SVM with SPR	78.11	79.36	78.1	78.09
Early Fusion	83.46	89.73	83.46	84.45
Late Fusion	83.96	85.31	83.96	83.92
EUIGR	80.66	83.11	80.66	78.65
GRfid	41.84	47.58	41.83	39.66

TABLE II: Accuracy (Acc.), Precision (Pre.), Recall (Rec.), and F1-score (F1) of methods using phase, RSS, and AoA.

Metric \ Method	Acc.	Pre.	Rec.	F1
RFC with SA	82.44	83.56	82.44	82.67
RFC with SWA	93.12	93.56	93.12	93.11
RFC with SPR	97.2	97.31	97.2	97.19
SVM with SA	79.13	81.38	79.12	79.52
SVM with SWA	91.09	91.23	91.09	91
SVM with SPR	93.12	93.39	93.12	93.08
Early Fusion	96.94	97.26	96.94	96.95
Late Fusion	95.92	96.21	95.92	95.86
EUIGR	95.41	95.76	95.41	95.39
GRfid	54.42	59.18	54.42	52.15

concatenating AoA features increases the model's accuracy to 93.12%.

In contrast with Early Fusion in TABLE. I, which achieves an accuracy of 83.46%, the same approach in TABLE. II (with AoA) shows a considerable improvement, reaching 96.94%. A similar trend is observed with Late Fusion, where the accuracy increases from 83.96% to 95.92%. While the EUIGR method shows an accuracy of 80.66%, it achieves 95.41% when AoA is incorporated. GRfid also benefits from AoA, with its performance increasing by almost 12%.

The normalized confusion matrices are shown in Fig 6 for models that use phase or a combination of phase and RSS as input features, and in Fig 7 for models that use AoA or its combination with phase and RSS. It can be observed that, while it is rare for any gesture to be classified with 100% accuracy across all methods in Fig 6, it frequently occurs that some gestures achieve perfect classification in certain methods when AoA tracking is utilized. Overall, incorporating AoA into phase and RSS signals or using AoA tracking alone considerably boosts the performance of gesture recognition systems.

## VI. Conclusion

In this work, we addressed the challenge of recognizing a large variety of hand gestures using passive reflective tags by introducing AoA tracking as a complementary feature to conventional RSS and phase-based methods. We showed that RSS and phase signals often lack the discriminative

power required for complex gesture differentiation due to signal similarity. By using AoA, which varies with hand movement, we were able to capture spatial information that enhanced the separability of gestures. Through the use of the MUSIC algorithm and Smart Antenna Switching (SAS), we demonstrated AoA estimation in static tag configurations. We then developed a Kalman smoothing-based AoA tracking algorithm for gesture execution. Our experiments confirmed that incorporating AoA features into gesture recognition pipelines leads to substantial improvements in classification accuracy, with gains of up to 15% in benchmark tests. These findings highlight the value of AoA as a robust and distinguishing feature for RF-based gesture recognition.

## References

- [1] R. Ghazalian, H. Chen, G. C. Alexandropoulos, G. Seco-Granados, H. Wyneersch, and R. Jäntti, "Joint user localization and location calibration of a hybrid reconfigurable intelligent surface," *IEEE Transactions on Vehicular Technology*, 2023.
- [2] S. Palipana, D. Salami, L. A. Leiva, and S. Sigg, "Pantomime: Mid-air gesture recognition with sparse millimeter-wave radar point clouds," *Proceedings of the ACM on Interactive, Mobile, Wearable and Ubiquitous Technologies*, vol. 5, no. 1, pp. 1–27, 2021.
- [3] X. Jiang, X. Gao, X. Wu, Q. J. Gu, and X. Liu, "Automatic RF leakage cancellation for improved remote vital sign detection using a low-if dual-pll radar system," *IEEE Transactions on Microwave Theory and Techniques*, 2023.
- [4] A. Alabsi, W. Gong, and A. Hawbani, "Emotion recognition based on wireless, physiological and audiovisual signals: A comprehensive survey," in *International conference on smart computing and cyber security: strategic foresight, security challenges and innovation*, pp. 121–138, Springer, 2021.
- [5] J. Xiao, B. Luo, L. Xu, B. Li, and Z. Chen, "A survey on application in rf signal," *Multimedia Tools and Applications*, pp. 1–24, 2023.
- [6] H. Landaluce, L. Arjona, A. Perallos, F. Falcone, I. Angulo, and F. Muralter, "A review of iot sensing applications and challenges using rfid and wireless sensor networks," *Sensors*, vol. 20, no. 9, p. 2495, 2020.
- [7] A. Haibi, K. Oufaska, K. El Yassini, M. Boulmalf, and M. Bouya, "Systematic mapping study on rfid technology," *IEEE Access*, vol. 10, pp. 6363–6380, 2022.
- [8] J. Xu, Z. Li, K. Zhang, J. Yang, N. Gao, Z. Zhang, et al., "The principle, methods and recent progress in rfid positioning techniques: A review," *IEEE Journal of Radio Frequency Identification*, 2023.
- [9] A. Florio, G. Avitabile, and G. Coviello, "Localization of rfid tags through real-time angle-of-arrival estimation," *IEEE Sensors Letters*, vol. 9, no. 3, pp. 1–4, 2025.
- [10] T. Faseth, M. Winkler, H. Arthaber, and G. Magerl, "The influence of multipath propagation on phase-based narrowband positioning principles in uhf rfid," in *2011 IEEE-APS Topical Conference on Antennas and Propagation in Wireless Communications*, pp. 1144–1147, IEEE, 2011.
- [11] J. S. Pereira, "Long-range rfid indoor positioning system for an autonomous wheelchair," *Sensors*, vol. 25, no. 8, p. 2542, 2025.
- [12] A. Fabris, O. K. Rayel, J. L. Rebelatto, G. L. Moritz, and R. D. Souza, "Aoa and rss-based ble indoor positioning system with kalman filter and data fusion," *IEEE Internet of Things Journal*, 2025.
- [13] Y. Zhang, Y. Wang, F. Li, W. Yu, C. Wang, and Y. Jiang, "Sign language recognition based on cnn-bilstm using rf signals," *IEEE Access*, 2024.
- [14] H. Xu, Y. Zhang, Z. Yang, H. Yan, and X. Wang, "Rf-csign: A chinese sign language recognition system based on large kernel convolution and normalization-based attention," *IEEE Access*, vol. 11, pp. 133767–133780, 2023.

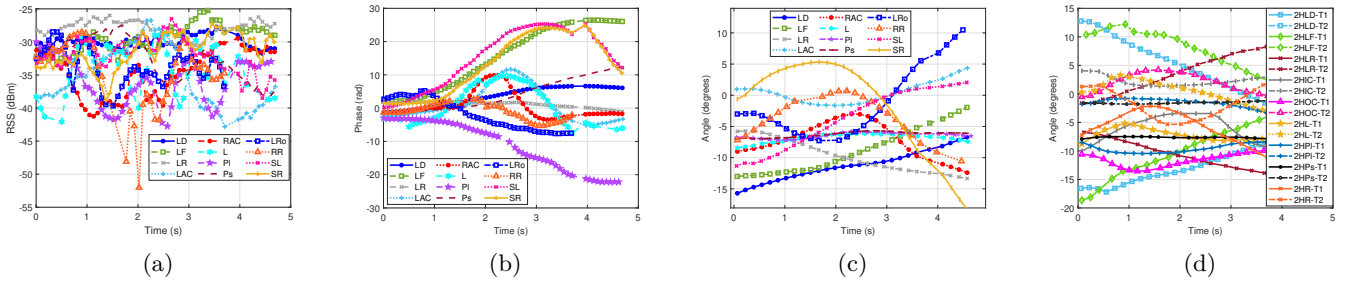


Fig. 5: Comparison of RSS, phase, and AoA features for gesture differentiation. (a) Processed RSS signals from the hand-mounted tag for a simple set of gestures. (b) Processed phase signals from the hand-mounted tag for a simple set of gestures. (c) Estimated AoA signals from the hand-mounted tag for a simple set of gestures. (d) Estimated AoA signals from the hand-mounted tags for a complex set of gestures. T1 and T2 denote Tag 1 and Tag 2, respectively.

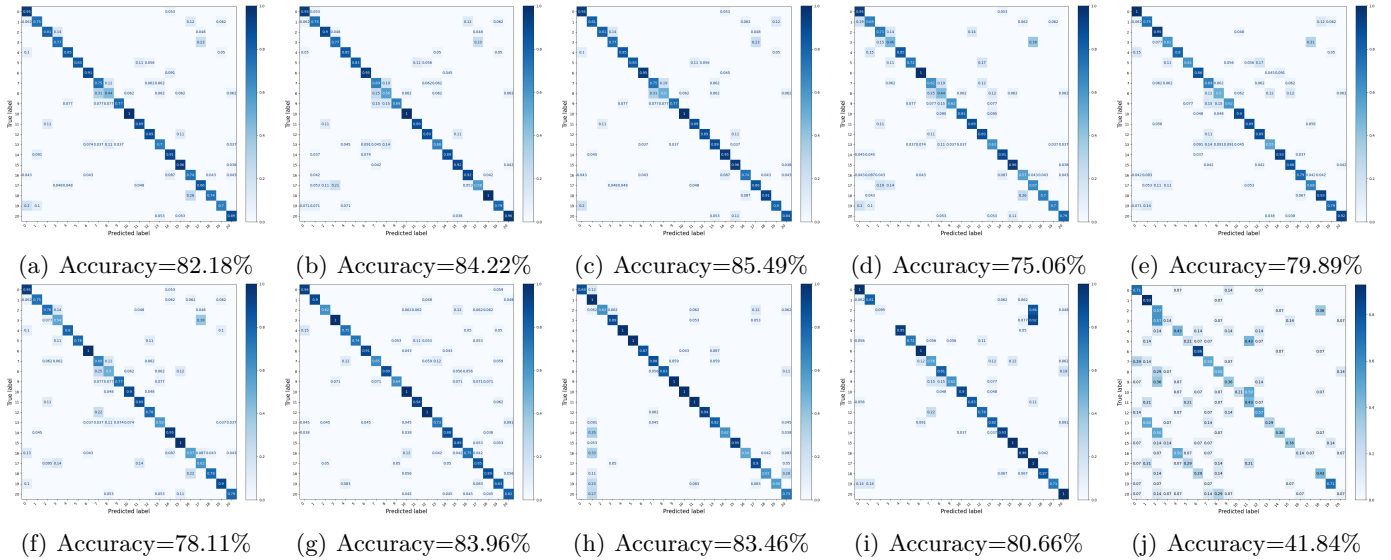


Fig. 6: Normalized confusion matrices obtained from models using phase, RSS, or both as input features: (a) RFC with SP; (b) RFC with SWP; (C) RFC with SPR; (d) SVM with SP; (e) SVM with SWP; (f) SVM with SPR; (g) Late Fusion; (h) Early Fusion; (i) EUIGR; (j) GRfid

- [15] C. Dian, D. Wang, Q. Zhang, R. Zhao, and Y. Yu, "Towards domain-independent complex and fine-grained gesture recognition with rfid," Proceedings of the ACM on Human-Computer Interaction, vol. 4, no. ISS, pp. 1–22, 2020.
- [16] M. Merenda, G. Cimino, R. Carotenuto, F. G. Della Corte, and D. Iero, "Edge machine learning techniques applied to rfid for device-free hand gesture recognition," IEEE Journal of Radio Frequency Identification, vol. 6, pp. 564–572, 2022.
- [17] S. Zhang, Z. Ma, C. Yang, X. Kui, X. Liu, W. Wang, J. Wang, and S. Guo, "Real-time and accurate gesture recognition with commercial rfid devices," IEEE Transactions on Mobile Computing, vol. 22, no. 12, pp. 7327–7342, 2022.
- [18] Y. Zou, J. Xiao, J. Han, K. Wu, Y. Li, and L. M. Ni, "Grfid: A device-free rfid-based gesture recognition system," IEEE Transactions on Mobile Computing, vol. 16, no. 2, pp. 381–393, 2016.
- [19] C. Wang, J. Liu, Y. Chen, H. Liu, L. Xie, W. Wang, B. He, and S. Lu, "Multi-touch in the air: Device-free finger tracking and gesture recognition via cots rfid," in IEEE INFOCOM 2018–IEEE conference on computer communications, pp. 1691–1699, IEEE, 2018.
- [20] Z. Ma, S. Zhang, J. Liu, X. Liu, W. Wang, J. Wang, and S. Guo, "Rf-siamese: Approaching accurate rfid gesture recognition with one sample," IEEE Transactions on Mobile Computing, vol. 23, no. 1, pp. 797–811, 2022.
- [21] S. D. Regani, B. Wang, Y. Hu, and K. R. Liu, "Gwrite: Enabling through-the-wall gesture writing recognition using wifi," IEEE Internet of Things Journal, vol. 10, no. 7, pp. 5977–5991, 2022.
- [22] Y. Yao, C. Zhao, Y. Pan, C. Sha, Y. Rao, and T. Wang, "Human gesture recognition based on ct-a hybrid deep learning model in wifi environment," IEEE Sensors Journal, 2023.
- [23] Y. Chen and X. Huang, "Wignn: Wifi-based cross-domain gesture recognition inspired by dynamic topology structure," IEEE Wireless Communications, 2024.
- [24] Y. Qin, S. Sigg, S. Pan, and Z. Li, "Direction-agnostic gesture recognition system using commercial wifi devices," Computer Communications, vol. 216, pp. 34–44, 2024.
- [25] Y. Gu, H. Yan, X. Zhang, Y. Wang, J. Huang, Y. Ji, and F. Ren, "Attention-based gesture recognition using commodity wifi devices," IEEE Sensors Journal, vol. 23, no. 9, pp. 9685–9696, 2023.
- [26] Y. Gu, X. Zhang, Y. Wang, M. Wang, H. Yan, Y. Ji, Z. Liu, J. Li, and M. Dong, "Wigrunt: Wifi-enabled gesture recognition using dual-attention network," IEEE transactions on human-machine systems, vol. 52, no. 4, pp. 736–746, 2022.
- [27] B. Jin, X. Ma, Z. Zhang, Z. Lian, and B. Wang, "Interference-robust millimeter-wave radar-based dynamic hand gesture recognition using 2d cnn-transformer networks," IEEE Internet of Things Journal, 2023.
- [28] J.-T. Yu, Y.-H. Tseng, and P.-H. Tseng, "A mmwave mimo radar-based gesture recognition using fusion of range, velocity, and angular information," IEEE Sensors Journal, 2024.
- [29] Y. Wu, X. Wang, S. Guo, B. Zhang, and G. Cui, "A lightweight

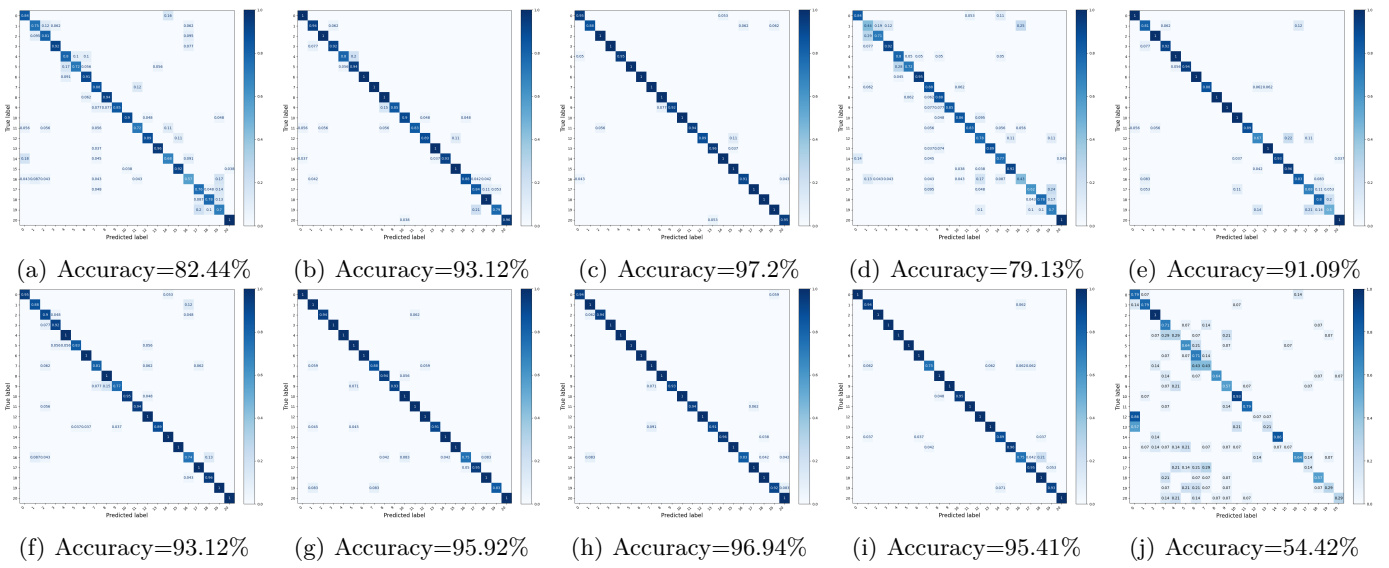


Fig. 7: Normalized confusion matrices obtained from models using phase, RSS, AoA, or their combinations as input features.: (a) RFC with SA; (b) RFC with SWA; (C) RFC with SPRA; (d) SVM with SA; (e) SVM with SWA; (f) SVM with SPRA; (g) Late Fusion; (h) Early Fusion; (i) EUIGR; (j) GRfid

network with multi-feature fusion for mmwave radar based hand gesture recognition,” IEEE Sensors Journal, 2024.

[30] C. Jin, X. Meng, X. Li, J. Wang, M. Pan, and Y. Fang, “Rodar: Robust gesture recognition based on mmwave radar under human activity interference,” IEEE Transactions on Mobile Computing, 2024.

[31] L. Qiao, Z. Wang, Y. Shu, B. Xiao, X. Luan, Y. Shi, W. Li, and X. Gao, “Simple and efficient gesture recognition based on frequency modulated continuous wave radar,” IEEE Transactions on Instrumentation and Measurement, 2024.

[32] D. Salami, R. Hasibi, S. Palipana, P. Popovski, T. Michoel, and S. Sigg, “Tesla-rapture: A lightweight gesture recognition system from mmwave radar sparse point clouds,” IEEE Transactions on Mobile Computing, vol. 22, no. 8, pp. 4946–4960, 2022.

[33] H. Li, C. Ye, and A. P. Sample, “Idsense: A human object interaction detection system based on passive uhf rfid,” in Proceedings of the 33rd Annual ACM Conference on Human Factors in Computing Systems, pp. 2555–2564, 2015.

[34] Z. Zhou, L. Shangguan, X. Zheng, L. Yang, and Y. Liu, “Design and implementation of an rfid-based customer shopping behavior mining system,” IEEE/ACM transactions on networking, vol. 25, no. 4, pp. 2405–2418, 2017.

[35] L. Shangguan, Z. Zhou, and K. Jamieson, “Enabling gesture-based interactions with objects,” in Proceedings of the 15th Annual International Conference on Mobile Systems, Applications, and Services, pp. 239–251, 2017.

[36] X. Li, Y. Zhang, I. Marsic, A. Sarcevic, and R. S. Burd, “Deep learning for rfid-based activity recognition,” in Proceedings of the 14th ACM Conference on Embedded Network Sensor Systems CD-ROM, pp. 164–175, 2016.

[37] Y. Bu, L. Xie, Y. Gong, C. Wang, L. Yang, J. Liu, and S. Lu, “Rf-dial: An rfid-based 2d human-computer interaction via tag array,” in IEEE INFOCOM 2018–IEEE conference on computer communications, pp. 837–845, IEEE, 2018.

[38] T. Salo, T. Vuohijoki, A. Shaikh, J. Virkki, and J. Vanhala, “Carbon nonwoven rfid antennas for smart wearable applications,” in 2024 IEEE International Conference on Flexible and Printable Sensors and Systems (FLEPS), pp. 1–4, IEEE, 2024.

[39] K. Kruse, W. Sauerwein, J. Lübben, and R. Dodel, “Smart technologies and textiles and their potential use and application in the care and support of elderly individuals: A systematic review,” Reviews on Advanced Materials Science, vol. 63, no. 1, p. 20230174, 2024.

[40] S. Golipoor and S. Sigg, “Accurate rf-sensing of complex gestures using rfid with variable phase-profiles,” in 2023 IEEE 32nd International Symposium on Industrial Electronics (ISIE), pp. 1–4, IEEE, 2023.

[41] S. Golipoor and S. Sigg, “Rfid-based human activity recognition using multimodal convolutional neural networks,” in 2024 IEEE 29th International Conference on Emerging Technologies and Factory Automation (ETFA), pp. 1–6, IEEE, 2024.

[42] K. Cheng, N. Ye, R. Malekian, and R. Wang, “In-air gesture interaction: Real time hand posture recognition using passive rfid tags,” IEEE access, vol. 7, pp. 94460–94472, 2019.

[43] L. Xie, C. Wang, A. X. Liu, J. Sun, and S. Lu, “Multi-touch in the air: Concurrent micromovement recognition using rf signals,” IEEE/ACM Transactions on Networking, vol. 26, no. 1, pp. 231–244, 2017.

[44] H. Zhang, L. Wang, J. Pei, F. Lyu, M. Li, and C. Liu, “Rf-sign: Position-independent sign language recognition using passive rfid tags,” IEEE Internet of Things Journal, 2023.

[45] R. H. Clarke, D. Twede, J. R. Tazelaar, and K. K. Boyer, “Radio frequency identification (rfid) performance: the effect of tag orientation and package contents,” Packaging Technology and Science: An International Journal, vol. 19, no. 1, pp. 45–54, 2006.

[46] D. Vasisht, G. Zhang, O. Abari, H.-M. Lu, J. Flanz, and D. Katabi, “In-body backscatter communication and localization,” in Proceedings of the 2018 Conference of the ACM Special Interest Group on Data Communication, pp. 132–146, 2018.

[47] Y. Yu, D. Wang, R. Zhao, and Q. Zhang, “Rfid based real-time recognition of ongoing gesture with adversarial learning,” in Proceedings of the 17th Conference on Embedded Networked Sensor Systems, pp. 298–310, 2019.

[48] S. Golipoor and S. Sigg, “Environment and person-independent gesture recognition with non-static rfid tags leveraging adaptive signal segmentation,” in 2024 IEEE 29th International Conference on Emerging Technologies and Factory Automation (ETFA), pp. 1–8, IEEE, 2024.

[49] S. Kulkarni, A. Thakur, S. Soni, A. Hiwale, M. H. Belsare, and A. B. Raj, “A comprehensive review of direction of arrival (doa) estimation techniques and algorithms,” Journal of Electronics and Electrical Engineering, pp. 138–186, 2025.

[50] G. K. Fischer, T. Schaechtle, A. Gabrielli, J. Bordoy, I. Häring, F. Höflinger, and S. J. Rupitsch, “A systematic survey and analysis of angular-based indoor localization and positioning,” Authorea Preprints, 2024.

[51] F. Mazhar, M. G. Khan, and B. Sällberg, “Precise indoor positioning using uwb: A review of methods, algorithms and implementations,” Wireless Personal Communications, vol. 97, no. 3, pp. 4467–4491, 2017.

[52] A. A. Abbas, M. El-Absi, A. Abualhijaa, K. Solbach, and T. Kaiser, “Dielectric resonator-based passive chipless tag with

angle-of-arrival sensing,” IEEE Transactions on Microwave Theory and Techniques, vol. 67, no. 5, pp. 2010–2017, 2019.

[53] J. Ali, A. Narbudowicz, K. Kaemarungsi, and S. Chalermwisutkul, “Dual-chip rfid tag for enhanced indoor localization of iot assets,” in 2023 17th European Conference on Antennas and Propagation (EuCAP), pp. 1–5, IEEE, 2023.

[54] A. Gil-Martínez, M. Poveda-García, D. Cañete-Rebenaque, and J. L. Gómez-Tornero, “Frequency-scanned monopulse antenna for rssi-based direction finding of uhf rfid tags,” IEEE Antennas and Wireless Propagation Letters, vol. 21, no. 1, pp. 158–162, 2021.

[55] J. Mitsugi and Y. Kawakita, “Simultaneous gen2 inventory and angle of arrival measurement of backscatter signals with multiple commodity sdrs,” IEEE Journal of Radio Frequency Identification, vol. 5, no. 4, pp. 368–377, 2021.

[56] K. Skyvalakis, E. Giannelos, E. Andrianakis, and A. Bletsas, “Elliptical doa estimation & localization,” IEEE Journal of Radio Frequency Identification, vol. 6, pp. 394–401, 2022.

[57] Y. Ma, B. Wang, S. Pei, Y. Zhang, S. Zhang, and J. Yu, “An indoor localization method based on aoa and pdoa using virtual stations in multipath and nlos environments for passive uhf rfid,” IEEE Access, vol. 6, pp. 31772–31782, 2018.

[58] X. Zhao, G. Wang, Z. An, Q. Pan, Q. Lin, and L. Yang, “Pushing the boundaries of high-precision aoa estimation with enhanced phase estimation protocol,” IEEE Internet of Things Journal, 2024.

[59] H. Liu, Z. Meng, J. Xu, C. Li, Z. Li, N. Gao, and Z. Zhang, “Simultaneous detection of the orientation and position of moving objects with simple rfid array for industrial iot applications,” IEEE Internet of Things Journal, 2024.

[60] Z. Wang, R. Li, R. Song, B. Christo, L. Sun, and Z. Lin, “Tri-aoa: Robust aoa estimation of mobile rfid tags with cots devices,” in GLOBECOM 2022-2022 IEEE Global Communications Conference, pp. 6451–6456, IEEE, 2022.

[61] L. Xie, Y. Ren, Y. Wang, W. Nie, and M. Zhou, “An aoa and orientation angle-based localization algorithm for passive rfid tag array,” Wireless Communications and Mobile Computing, vol. 2022, no. 1, p. 7774166, 2022.

[62] Z. Wang, J. A. Zhang, F. Xiao, and M. Xu, “Accurate aoa estimation for rfid tag array with mutual coupling,” IEEE Internet of Things Journal, vol. 9, no. 15, pp. 12954–12972, 2022.

[63] A. Gil-Martínez, M. Poveda-García, J. García-Fernández, M. M. Campo-Valera, D. Cañete-Rebenaque, and J. L. G. Tornero, “Direction finding of rfid tags in uhf band using a passive beam-scanning leaky-wave antenna,” IEEE Journal of Radio Frequency Identification, vol. 6, pp. 552–563, 2022.

[64] C. Yang, X. Wang, and S. Mao, “Rfid tag localization with a sparse tag array,” IEEE internet of things journal, vol. 9, no. 18, pp. 16976–16989, 2021.

[65] J. Sherman, “Properties of focused apertures in the Fresnel region,” IRE Transactions on Antennas and Propagation, vol. 10, no. 4, pp. 399–408, 1962.

[66] Impinj, “Impinj speedway revolution reader r420 datasheet.” <https://www.dipolrfid.com/files/archivosproductos/10/Data sheet-Impinj-Speedway-Revolution-Reader-R420-RFID-UHF.pdf\protect\penalty\z@>, 2025. [Online].

[67] A. Aiouaz, P. Dietrich, D. Ord, and O. Khwaja, “RFID readers and systems with antenna switching upon detecting too few tags and methods,” Feb. 21 2012. US Patent 8,120,494.

[68] R. Schmidt, “Multiple emitter location and signal parameter estimation,” IEEE transactions on antennas and propagation, vol. 34, no. 3, pp. 276–280, 1986.

[69] H. W. Sorenson, “Least-squares estimation: from gauss to kalman,” IEEE spectrum, vol. 7, no. 7, pp. 63–68, 1970.

[70] S. Särkkä and L. Svensson, Bayesian filtering and smoothing, vol. 17. Cambridge university press, 2023.

[71] Impinj, “Getting started with impinj speedway connect on reader software.” <https://support.impinj.com/hc/en-us/articles/360000042780-Getting-Started-with-Impinj-Speedway-Connect-on-reader-software>, 2025. [Online].

[72] C. Cortes and V. Vapnik, “Support-vector networks,” Machine learning, vol. 20, no. 3, pp. 273–297, 1995.

[73] F. M. Calatrava-Nicolás and O. M. Mozos, “Light residual network for human activity recognition using wearable sensor data,” IEEE Sensors Letters, 2023.